UC Davis
UC Davis Previously Published Works

Title
Coarse-grained modeling of polystyrene-modified CNTs and their interactions with lipid bilayers

Permalink
https://escholarship.org/uc/item/25v243x1

Journal
Biophysical Journal, 122(10)

ISSN
0006-3495

Authors
Gul, Gulsah
Faller, Roland
Ileri-Ercan, Nazar

Publication Date
2023-05-01

DOI
10.1016/j.bpj.2023.04.005

Copyright Information

Peer reviewed

Coarse-Grained Modeling of Polystyrene-Terminated CNTs and Their Interactions with Lipid Bilayers

Gulsah Gul,*,† Roland Faller,† Nazar Ileri-Ercan*

*Department of Chemical Engineering, Bogazici University, Bebek, Istanbul, Turkey

†Department of Chemical Engineering, University of California, Davis, CA, United States

Abstract

In the present work, we describe Martini3 coarse-grained (CG) models of polystyrene (PS) and carboxyl-terminated polystyrene (PSCOOH) functionalized carbon nanotubes (CNTs) and investigate their interactions with lipid bilayers with and without cholesterol (CHOL) using molecular dynamics (MD) simulations. By changing the polystyrene chain length and grafting density at the end ring of the CNTs at two different nanotube concentrations, we observe the translocation of nanoparticles as well as changes in the lipid bilayer properties. Our results show that all developed models passively diffuse into the membranes without causing any damage to the membrane integrity although high concentrations of CNTs induce structural and elastic changes in lipid bilayers. In the presence of CHOL, increasing CNT concentration results in decreased rates of CHOL transmembrane motions. On the other hand, CNTs are prone to lipid and polystyrene blockage which affects their equilibrated configurations, and tilting behavior within the membranes. Hence, we demonstrate that polystyrene functionalized CNTs are promising drug-carrier agents. However, polystyrene chain length and grafting density are important factors to consider to enhance the efficiency of drug delivery.

Keywords: Carbon nanotubes, polystyrene functionalization, lipid bilayer, molecular dynamics

Statement of Significance

Coarse-grained Martini3 models of PS and PSCOOH functionalized CNTs were developed and their interactions with lipid bilayers were investigated. Our results show that:

- High concentrations of CNTs induce structural and elastic changes in lipid bilayers. Yet, all models passively diffuse into the membranes with no damage to the membrane integrity.
- Increasing CNT concentration results in decreased CHOL transmembrane motion rate.
- CNTs are prone to lipid and polystyrene blockage affecting their equilibrated configurations and tilting behavior within the membranes.

Introduction

Single-walled carbon nanotubes (SWCNTs) have attracted much attention due to their superior electronic, optical, and mechanical properties along with their chemical stability.[1-5] In particular, the ability of CNTs to readily cross the cell membrane together with their capacity to transport a large number of molecules has triggered the design of nanotube-based delivery systems.[6-8] In these systems, CNTs have been used as antitumor therapeutics and molecular carriers to the cells through the addition or loading of drugs,[9-11] genes,[12] and proteins.[13,14] The efficient delivery of such systems into cells requires low cytotoxicity, high solubility, and a long blood circulation lifetime. However, CNTs are insoluble in most common solvents, including water, and the hydrophobic nature of CNTs limits their use as carriers due to their aggregation in aqueous media under physiological conditions. The accumulation of CNTs in cells, tissues, or organs can result in harmful effects such as toxicity.[15] To overcome this, CNTs have been covalently or noncovalently functionalized with amphiphilic or hydrophilic molecules including lipids, proteins, surfactants, and polymers.[16-20]

Previous experimental and computational studies have mainly focused on the polyethylene glycol (PEG) modification of nanotubes.[21] Both covalent conjugation with PEG and non-covalent wrapping with PEGylated lipids have provided a long blood circulation half-life, delayed clearance, and low toxicity *in vitro* and *in vivo*.[22-25] To increase the circulation lifetime and the organ uptake and to decrease the accumulation of nanotubes, the length and the density of PEG chains were optimized, and relatively low accumulation in the reticuloendothelial system was recorded with the optimal blood circulation half-life of 12-13 h for SWCNTs.[26] Similarly, by

coating CNTs with polymers, ultralong blood circulation of about 22 hr was obtained in mice.[24] Computer simulations, on the other hand, have played a significant role in studying the energetics and mechanics of how nanotubes penetrate through the cell membrane and the impact on lipid structures, CNT properties, and surface functional groups.[27-32] PEG modification of CNTs has been investigated both by atomistic and coarse-grained molecular dynamics (CGMD) simulations in terms of polymer chain length and grafting density.[33,34] It has been revealed that PEG chains exhibit similar conformations as experimentally observed, i.e., mushroom-to-brush transition, in agreement with the Alexander–de Gennes theory.[34]

Studies on polystyrene functionalization of CNTs have demonstrated that polystyrene modification increases the solubility of CNTs in various solvents and facilitates their dispersion.[35-38] Furthermore, the mechanical properties, such as Young's Modulus, shear stress, etc., significantly improve by the dispersion of CNTs in polystyrene matrices.[36, 39, 40] However, polystyrene-coated CNTs have rarely been studied for their toxicity, despite their improved performances. To our knowledge, the only study conducted in this context involved coating multi-walled carbon nanotubes (MWCNTs) with polystyrene-based polymers, which has shown that polystyrene-functionalized MWCNTs reduce oxidative stress and inflammation both *in vitro* and *in vivo* and do not lead to pulmonary toxicity.[41] Similarly, we found by data mining[42] and atomistic MD simulations[43] that polystyrene coating could be an alternative route for the safe and efficient delivery of drugs via CNTs. Now, we extend our observations by developing the CG Martini3 models of pristine SWCNTs and functionalized SWCNTs through MD simulations and examine the effect of polystyrene functionalization as well as the carboxyl termination in polystyrene on the translocation of SWCNTs. Our models have been validated by the free energy partitioning behavior of the nanotubes observed in all-atom simulations and experiments and give an insight into the interactions of polystyrene-modified CNTs with lipid bilayers in the absence and presence of CHOL.

Methods

We used CGMD simulations to study the interactions between pristine/functionalized CNTs and lipid bilayer systems. Lipid membranes were formed from 1-palmitoyl-2-oleoyl-sn-glycero-3-phosphocholine (POPC) and CHOL. Free energy simulations were performed with GROMACS 2020 while other MD simulations are performed with GROMACS 2021.3.[44] Visual Molecular Dynamics (VMD) software[45] was used for visualization purposes.

    1. **Coarse-Graining Methodology**

Atomistic Reference Simulations: Initial configurations were generated in the CHARMM-GUI[46] and a detailed setup procedure was described previously.[43] SWCNTs with the chirality of (18,0) were in ~1.4 nm diameter and ~3 nm C-to-C length, and polystyrene chains consisted of 29 monomers (~3 kDa) in atactic form. Polystyrene was covalently attached to CNT with an amide linker as described in experimental studies.[37,38,47,48] CHARMM-compatible INTERFACE (IFF) force field[49] was used for the nanotube model while CGenFF 4.5[50] was used for the linker. The partial charges and bonded parameters of modified CNT can be found at the Supporting Material. The pristine and functionalized nanotube systems were solvated in TIP3P water and included 6673 and 27561 water molecules, respectively. After the steepest descent algorithm minimization, the constant particle number, volume, and temperature (NVT) equilibration was applied for 5 ns with 1 fs timestep. The temperature was maintained at 310 K by velocity rescaling thermostat[51] with a time constant of 1.0 ps. Non-bonded interactions were cut off at the 1.2 nm distance and van der Waals interactions were switched off between 1.0 and 1.2 nm by the force-switch modifier. The long-range electrostatic interactions were treated with the particle mesh Ewald (PME) algorithm.[52] Pressure was controlled at 1 bar in an isotropic fashion by the Parrinello–Rahman barostat[53] with a coupling constant of 5 ps and a compressibility factor of 4.5 x 10^{-5} bar^{-1}. The system with pristine CNT was simulated for 50 ns, while the one with polystyrene functionalized CNT was simulated for 100 ns with 2 fs timestep in the constant particle number, pressure, and temperature (NPT) ensemble. During the simulations, hydrogens were constrained through the LINCS algorithm[54].

CG Modelling of CNT: In CGMD simulations, especially for phospholipid membrane systems, Martini force field parameters have been widely used.[55] Recently a new version of Martini, Martini3, has been proposed with significant improvements in bead types and interaction levels which make more versatile and accurate predictions of realistic systems.[56] Therefore, we adopted the Martini3 parameterization procedure for the CNT.[57] By using our atomistic reference simulation results, we applied 2-to-1 mapping to consecutive C beads in the same ring of SWCNTs via the CGBuilder tool (https://jbarnoud.github.io/cgbuilder/).[58] Thus, end group beads (H-bonding) were represented with TC5 bead type (which corresponds to benzene ring beads) while others are represented with TC5e (which corresponds to naphthalene ring beads). The bonded interactions between neighbor beads were obtained from atomistic simulations and force constants of 50000 kJ mol^{-1} and 1500 kJ mol^{-1} rad^{-2} (which were obtained by trial-and-error procedure) were used to capture the equilibrium bond lengths and bond angles, respectively. Also, the stiffness of the SWCNTs was provided through improper dihedral angles between two

intersecting planes with a force constant of 1000 kJ mol^{-1} rad^{-2}. The mapping scheme is demonstrated in Figure 1 with bonded interactions.
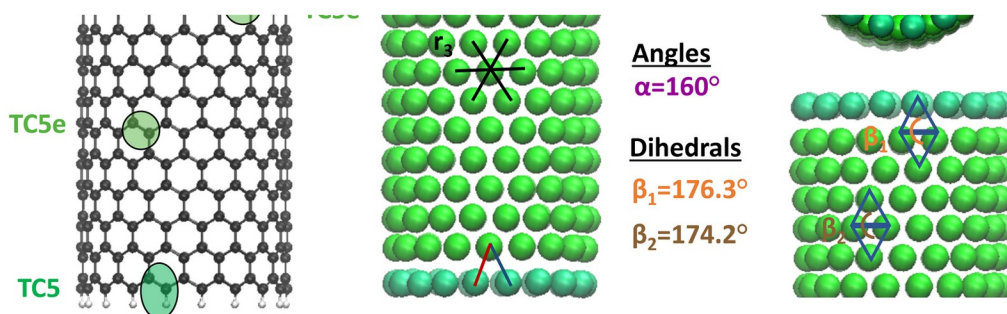
Figure 1. Martini3 coarse-grained modeling of CNT (18,0). The end rings of tubes are demonstrated in TC5 bead type while inner rings are TC5e. The bonded parameters, i.e., bonds, angles, and dihedrals are color-coded.

CG Modelling of PS and PSCOOH functionalized CNT: For the CG model, Martini3 parameters of polystyrene were obtained from the *polyply.py* script.[59] Polystyrene chains are covalently linked to the end ring of the nanotube by an amide linker, which was represented by one bead. Carboxyl modification was applied to the open end of the polystyrene ring. The amide linker and carboxyl group were represented with a polar P3 bead. However, only for the carboxyl bead, the Lennard-Jones interaction parameter (epsilon) was reduced (with a trial-and-error procedure) to 3.0 kJ/mol between P3 and W beads to obtain correct free energy partitioning behavior. Two bonds and three angles were defined between the nanotube-linker-polystyrene beads at the connection point. The bonded parameters reflected the atomistic symmetry, and the mapping scheme is demonstrated in Figure 2. However, it should be noted that the bonded

parameters change with respect to the CNT diameter and polystyrene chain length, and therefore, optimization may be required for different systems. The bonded parameters between the PS and carboxyl group, on the other hand, were assumed to be the same as the parameters of a continuing chain of PS [60] as shown in Figure S1. The corresponding force field files are available at the Supporting Material.

Bonds
r_1=0.23 nm
r_2=0.24 nm

Angles
α_1=101°
α_2=151°
α_3=150°
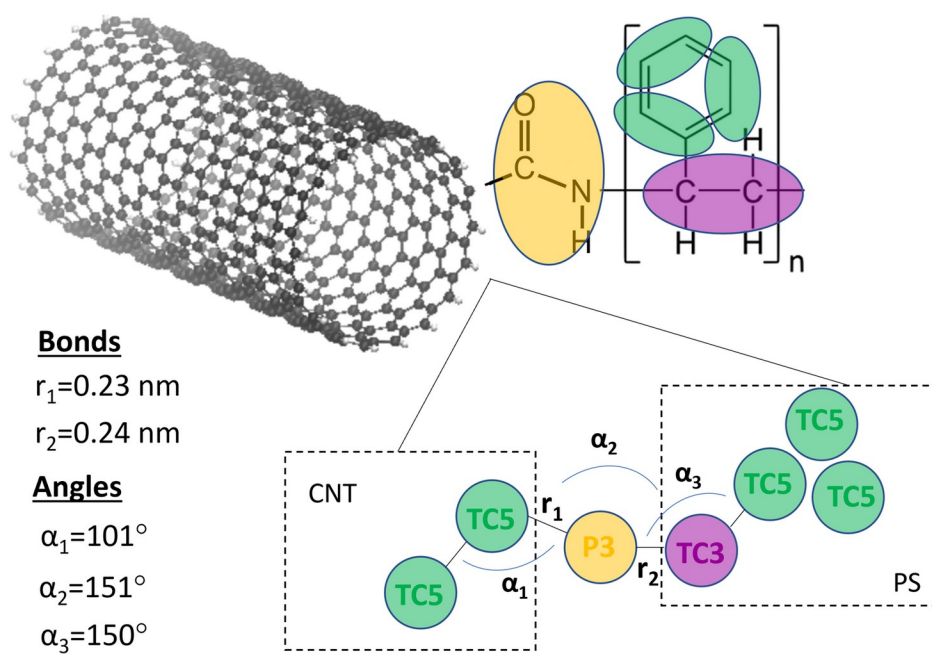
Figure 2. Martini3 coarse-grained modeling of PS-functionalized CNT (18,0). The linker is demonstrated by the P3 bead type, and the bonded parameters at the connection point are listed on the left.

CG Simulation Parameters: The mapped SWCNT configuration was solvated with SPC water in a box where the solute-to-box edge distance is 4 nm. After the steepest descent minimization, equilibration was done for 30 ns with 10 fs timestep in the NPT ensemble to relax the system. During equilibration, isotropic pressure coupling was applied to keep the pressure at 1 bar with Berendsen barostat[61] with a coupling constant of 5 ps. The temperature was maintained at 310 K by velocity rescale thermostat[51] with a time constant of 1.0 ps. Non-bonded interactions were cut

off at a 1.2 nm distance. The Lennard-Jones interactions were shifted with the Potential-Shift-Verlet modifier while the Coulomb potential was modeled using the Reaction Field scheme[62,63] with a permittivity constant of $\varepsilon_r = 15$. The pressure of the system was set to 1 bar using a Parrinello–Rahman barostat[53] with a coupling constant of 5 ps and a compressibility factor of 3 x 10^{-4} bar^{-1}. NPT production runs took 1 μs and half the simulation time was used for the analysis.

Free Energy Simulations: Free energies of solvation were calculated through the thermodynamic integration (TI) method using Bennett's Acceptance Ratio[64] which is based on the numerical integration of the derivative of Hamiltonian with respect to the coupling parameter λ:[65]

$$\Delta G = \int_{\lambda=0}^{\lambda=1} \left\langle \frac{\partial H(\lambda)}{\partial \lambda} \right\rangle_\lambda d\lambda \tag{1}$$

Then the free energy of transfer was calculated from the difference in the free energy of solvation values in water and octanol solvents:

$$\Delta G_{transfer} = \Delta G_{octanol} - \Delta G_{water} \tag{2}$$

To reduce the simulation costs, a small CNT with (6,0) chirality and ~1.5 nm length was used with 5 monomers of PS (~0.5 kDa). For pristine SWCNTs, only van der Waals interactions were coupled between $\lambda = 0$ (interactions were off) and $\lambda = 1$ (interactions were on) since SWCNT has no partial charges. For functionalized SWCNTs, both van der Waals and Coulomb interactions were coupled sequentially. The λ values were equally spaced and identical in each simulation. Therefore, we obtained 10 and 20 runs for pristine and functionalized SWCNTs, respectively. In the all-atom run, 1 ns of NVT and 4 ns of NPT equilibration were applied before a 50 ns NPT production run. The stochastic dynamics integrator with 2 fs of timestep was used in all simulations and the temperature was set to 298 K. The pressure was controlled at 1 bar by using Parrinello-Rahman barostat[53] with a time constant of 1 ps. Non-bonded interaction cutoff values were set to 1.2 nm. The PME algorithm[52] was used for the calculation of long-range electrostatic interactions with a sixth-order spline interpolation and a 0.12 nm grid spacing. To remove the singularity in the potentials, a soft-core potential was used[66] with the soft-core parameter of 0.5 and the soft-core power of 1. For CG simulations, the same parameters in the 'CG Simulation Parameters' section were used with the pressure coupling constant of 4 ps, and 1 μs of production run followed 50 ns of equilibration with the stochastic integrator at 298 K.

Potential of Mean Force (PMF) Simulations: PMF calculations were performed to investigate the transfer of CNT across the lipid bilayer by the umbrella sampling method.[67] In all-atom simulations, the POPC bilayer which consists of 128 lipids was used with our smaller nanotube model (D = ~0.5 nm, L= ~1.5 nm). The nanoparticle was placed ~3.75 nm away from the z-coordinate of the bilayer center-of-mass (COM). Once the system was equilibrated for 5 ns, the nanoparticle was pulled through the center of the bilayer at 0.1 nm intervals. The distance between the COM of the nanoparticle and the membrane was restrained in the z-direction with a harmonic potential force constant of 1000 kJ mol^{-1}. Each all-atom umbrella window was simulated for 50 ns (10 ns extracted for equilibration) under the NPT ensemble at 310 K with a total simulation time of ~2 μs for 38 independent windows. For CG simulations, the same procedure was followed with CNT (6,0) over 256 lipids of POPC. Each CG umbrella window was simulated for 1 μs (200 ns extracted for equilibration) under the NPT ensemble at 310 K with a total simulation time of ~40 μs. Other simulation parameters are given in the 'Atomistic' and 'CG Simulation Parameters' sections. The pressure was coupled semi-isotropically. The analysis of the umbrella simulations was performed using the weighted histogram analysis method (WHAM).[68,69]

2. Interaction of CNTs with Lipid Bilayers at CG Level

CNT (18,0) was covalently linked to PS or PSCOOH, which has 29 (~3 kDa), 48 (~5 kDa), or 96 (~10 kDa) monomers. The grafting density in the end ring of CNT was determined as zero, one, or evenly distributed two, four, or six chains of PS/PSCOOH with 29 monomers (c.f. Figure S2). Two model membranes, POPC only and POPC with 30 % CHOL, were constructed by CHARMM-GUI.[46] To reflect the realistic biological environment, 2048 lipids were solvated in 48401 and 49571 CG waters for POPC and POPC/CHOL systems, respectively, in 0.15 M NaCl. Each membrane system was simulated in the absence of nanoparticles, and the presence of 1 and 5 nanoparticles. Initially, the nanoparticles were equilibrated in water for 1 μs under the NPT ensemble, then the resultant configurations were placed vertically about ~2 nm away from the headgroups of the equilibrated bilayer in the z-direction. After a short equilibration, the systems were simulated in the NPT ensemble for 10 μs with a 20 fs timestep using Martini3 parameters.[56]

Validation of CHOL Parameters: The preliminary version of the Martini 3 CHOL model was provided by Dr. Paulo C. T. Souza and can be obtained upon request from him (paulocts@gmail.com) or from Dr. Siewert J. Marrink (s.j.marrink@rug.nl). We validated this model by comparing it with atomistic and Martini2 parameters after changing the CHOL content

between 0-50 % in POPC lipid systems. Results for the area-per-lipid (APL), bilayer thicknesses, and order parameters are available in Figure S5 and Figure S6.

MD Analysis: The membrane properties and the interactions of pristine and functionalized CNTs with the membrane were evaluated through the APL, lipid bilayer thickness, density distribution, lipid tail order parameters, diffusion constants, and CHOL flip-flop rates. APL values were obtained through Voronoi Tessellation by FATSLIM script.[70] The bilayer thickness was found by calculating the center-of-mass distance of PO4 beads in the z-direction from the upper leaflet to the lower leaflet. This calculation is done by using both *gmx distance* and LiPyphilic[71] module of Python[72] which are based on the mean distance in between PO4 beads in the upper and lower leaflets. However the results are listed in a single column as both produced the same results. To characterize the orientation of the lipids, the lipid tail order parameter was calculated by the *do-order-gmx5.py* script which is based on the equation:

$$S = \frac{3}{2} \langle \cos^2 \theta \rangle - \frac{1}{2} \tag{3}$$

where θ is the angle between the bilayer normal and the vector along a particular bond in a lipid tail. Here, S = 1, −0.5, and 0 indicate perfect alignment with the bilayer surface, an antialignment, and random orientation, respectively.[73]

The lateral mean square displacement (MSD) of lipids was extracted for PO4 and ROH beads of POPC and CHOL, respectively. After removing the system center of mass motion, diffusion coefficient values were calculated on MATLAB[74] by fitting the MSD versus time to the linear region of the line: MSD(t) = 4Dt + c where the constant c shows the offset at t= 0.[73]

To identify CHOL flip-flops, the translocation of ROH beads between the leaflets was monitored by the LiPyphilic[71] module of Python.[72] A CHOL molecule was assigned to a leaflet based on its minimum distance to the leaflet and if the distance is within 1 nm of neither or both leaflets, it was assigned to the midplane. A flip-flop event was defined as successful if the translocation from one leaflet to another follows by residing in the second leaflet for at least 100 frames (which corresponds to 10 ns simulation time). To calculate the flip-flop rate of CHOL, the total number of successful flip-flop events was divided into the number of CHOL and total simulation time.

Results

Validation of CNT Models: Martini2 CG models of CNT were previously developed by different groups,[31,75] but recently Martini3 force field has been introduced,[56] where the structural and thermodynamic properties of molecules are better represented. Therefore, we adopted the Martini3 small molecule parameterization procedure[57] to obtain more reliable models of pristine and functionalized CNTs. This parameterization relies on the distributions of bonded interactions in atomistic simulations, while non-bonded interactions are tuned to reproduce the free energies of transfer of the target molecules between aqueous and organic phases. The mapping strategy is based on the center-of-geometry (COG) approach, which takes into account the hydrogen atoms in addition to heavy atoms, i.e., carbon, oxygen, and nitrogen. The bonded parameters, i.e., bonds, angles, and dihedrals of CNTs, are derived from atomistic reference simulations and the distributions between AA and CG models are presented in Figures S3 and S4.

The non-bonded interactions obtained from atomistic and CG simulations are compared by calculating the free energy of solvation values and partition coefficients. Partition coefficient, which is represented as logP, is proportional to the free energy of transfer between two immiscible solvents and found by:[76]

$$logP = \frac{-\Delta G_{transfer}}{RTln(10)} \qquad (4)$$

where R is the gas constant, and T is the temperature, 298 K in this work.

From Table 1, the transfer free energy of -115.1 kJ/mol shows good agreement with less than 5 % error compared to the atomistic case. In literature, hydration, and solvation free energies of CNTs have been calculated by MD simulations[77,78] but the values are not comparable due to different sizes and configurations. Furthermore, the partitioning behavior of CNT from water to octanol has been previously modeled with its chiral vector by using solubility data.[79,80] We extracted the partition coefficient values from these proposed models and obtained less than a 10 % difference with a similar-sized CNT (6,0).

Table 1. Free energies of CNT (6,0) in water and octanol with calculated partition coefficients for all-atom (AA) and coarse-grained (CG) simulations. Reference partition coefficient values were calculated by the proposed models based on chiral vectors in the corresponding articles.

|	ΔG_{water} (kJ/mol)	$\Delta G_{octanol}$ (kJ/mol)	$\Delta G_{transfer}$ (kJ/mol)	logP	logP [ref]
AA	-48.9 ± 0.7	-168.9 ± 0.6	-120.0	21.0	18.7 [toropov],
CG	-54.9 ± 0.0	-170.0 ± 0.0	-115.1	20.2	19.2 [torrens]

For PS or PSCOOH functionalized CNTs, the free energy of transfer values are listed in Table 2. The negative estimates of free energies are in line with our previous findings and the high negative free energy of CNTs indicates the increased affinity of CNTs for water with functional groups.

Table 2. Free energies of transfer of PSCNT and PSCOOHCNT in water and octanol with calculated partition coefficients for all-atom (AA) and coarse-grained (CG) simulations. Here CNT is 1.5 nm in length with (6,0) chirality and the polystyrene chain consists of 5 monomers.

	$\Delta G_{transfer}$ (kJ/mol)	logP

PSCNT	**AA**	-153.5	26.9
	CG	-144.8	25.4
PSCOOHCNT	**AA**	-155.1	27.2
	CG	-144.2	25.2

To further validate the Martini3 CNT model, we calculated the PMF for a single CNT as a function of the distance from the center of the POPC bilayer (cf. Figure 3). The depth and the location of the free energy minimum, the free energy of the system when CNT is at the center of the bilayer (~-105 kJ/mol for AA and ~-120 kJ/mol for CG), and the slope of the PMF lines are similar in the two presentations. In CG simulations, the position of free energy minimum is at about 0.7 nm with an energy value of ~-125 kJ/mol while in AA simulations it is between ~0.7-0.9 with a slightly higher energy value. Since CG models are approximate, the results found here are in the reasonable range.
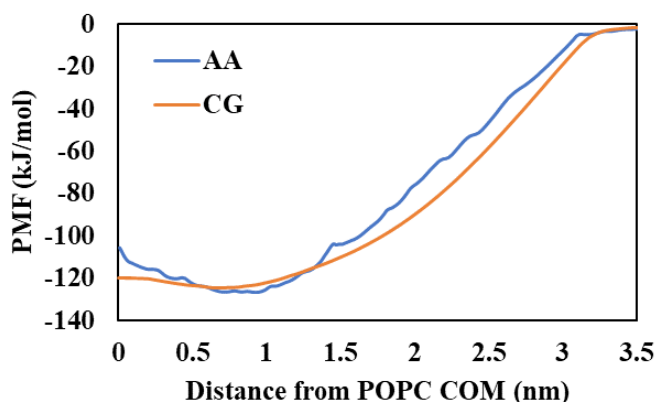
Figure 3. PMF change with the distance of the centers of masses of a single CNT (6,0) and a POPC bilayer.

Interaction of CNT Models with Lipid Bilayers: CNTs spontaneously diffuse into the membranes as reported elsewhere.[29,30,81] In homogeneous bilayers which consist of a single lipid component, the APL can be calculated simply by dividing the average box area into half the lipid number. However, this method is not suitable for heterogeneous bilayers containing various types of lipids of different sizes, such as CHOL. One way of calculating APL for mixed systems is to use Voronoi diagrams which rely on the projected area of lipids.[70] Therefore, we calculated the APL values with the latter method and presented the results in Table 3. The computed APL values for POPC only and POPC with 30% CHOL systems are 0.66 and 0.52 nm^2, respectively and in good agreement with the experimental and computational ranges of ~0.64-0.68 nm^2 for

POPC [82-84] and ~0.49 nm^2 for POPC/CHOL.[85] The surface area of a CHOL-included membrane is lower due to the condensing effect of CHOL.[86,87] Therefore, the APL values are lower for CHOL-included POPC than pure POPC as expected. Also, the change in APL values in the presence of a single pristine or functionalized CNT is small. In the presence of 5 functionalized CNTs for POPC and POPC/CHOL systems, there is a ~2% and ~3% increase in APL values, respectively.

The bilayer thickness of POPC and POPC/CHOL bilayers are calculated as 3.85 and 4.04 nm consistent with the experimental and computational values between ~ 3.70 - 3.92 nm [82-84] and ~ 4.4 - 4.5 nm, respectively.[85,88] While these values remain almost constant in the presence of a single nanoparticle, the thickness increases in systems containing 5 nanoparticles. Especially in POPC/CHOL systems, functionalized CNTs with 6 chains of PS or PSCOOH result in a ~10% increase in thickness because of the dense clustering of CNTs (c.f. Figure 6). In the presence of 5 functionalized CNTs, APL and thickness values are found to be very similar to either 4 or 6 chains of PS and PSCOOH.

The average carbon tail order parameters of POPC and POPC/CHOL are computed as ~0.35 and ~0.4, respectively (Table 3), which are higher than the experimental[88] and atomistic studies.[84] However, these values are in good agreement with previous Martini models.[89,90] Order parameters are not affected much by the introduction of nanoparticles in POPC, however, CHOL increases ordering in both systems. The clustering of CNTs with 4 chains of either PS or PSCOOH in the POPC/CHOL bilayer makes the ordering of lipid tails more pronounced and compact. The diffusion coefficient estimates in CG simulations are 2 to 10 times faster than their experimental counterparts. Therefore, the lateral diffusion coefficients of PO4 beads in POPC and POPC/CHOL are found as ~72 μm^2/s and ~47 μm^2/s which are larger than the experimental diffusivity of POPC at 15.3 μm^2/s [91] as expected. On the other hand, the diffusion constant of PO4 in POPC is ~1.5 times that of POPC with 30 % CHOL, which is consistent with experimental findings.[91,92] It has been observed that POPC/CHOL bilayers are in the liquid-disordered phase above 25 °C at all CHOL concentrations and lipid lateral diffusivity constants decrease in a linear relationship with increasing CHOL content.[92] Furthermore, the presence of a single pristine or functionalized CNT in the POPC bilayer reduces the lateral diffusivities by about 10 % while the presence of 5 functionalized CNTs decreases the diffusivities by about 20 %. This reduction reaches almost 50 % of that of POPC diffusivity with 5 PSCNT or PSCOOHCNT in the POPC/CHOL bilayers. On the other hand, the lateral diffusion coefficient of ROH beads in the POPC/CHOL bilayer is calculated as ~82 μm^2/s and decreases by about 7-15 % with the

increasing concentration of nanoparticles. Hence, the addition of 5 functionalized CNTs reduces the lateral diffusivities of POPC and CHOL, in the same manner.

Table 3. Area-per-lipid (APL), bilayer thickness, tail order parameter, and lateral diffusion coefficients of POPC and POPC/CHOL bilayers in the presence and absence of pristine and functionalized CNTs. Lateral diffusion coefficients represent the diffusivities of PO4 beads for POPC and ROH beads for CHOL, and standard errors are obtained through the regression of MSDs. Order parameters show the average tail order of both chains in POPC. Here NP, PS, and PSCOOH denote nanoparticle, polystyrene, and carboxyl-terminated polystyrene, respectively. The numbers next to 'PS' and 'PSCOOH' show the chain length while the ones after 'x' show the number of chains.

Model	No of NP	APL (nm²)	Bilayer Thickness (nm)	Order Parameter	Lateral Diffusion Coefficient (µm²/s)	
					PO4	ROH
POPC	-	0.661 ± 0.003	3.85 ± 0.01	0.346	71.8 ± 0.04	-
POPC-CNT	1	0.661 ± 0.003	3.86 ± 0.01	0.349	66.1 ± 0.09	-
POPC-PS29CNT	1	0.662 ± 0.003	3.86 ± 0.01	0.349	64.7 ± 0.02	-
POPC-PS48CNT	1	0.663 ± 0.003	3.86 ± 0.01	0.348	65.1 ± 0.04	-
POPC-PS96CNT	1	0.664 ± 0.003	3.86 ± 0.01	0.347	73.7 ± 0.03	-
POPC-PSCOOH29CNT	1	0.662 ± 0.003	3.86 ± 0.01	0.349	69.4 ± 0.05	-
POPC-PSCOOH48CNT	1	0.663 ± 0.003	3.86 ± 0.01	0.348	64.7 ± 0.05	-
POPC-PSCOOH96CNT	1	0.664 ± 0.003	3.86 ± 0.01	0.345	70.0 ± 0.03	-
POPC-PS29x2/CNT	1	0.663 ± 0.003	3.85 ± 0.01	0.348	64.7 ± 0.04	-
POPC-PS29x4/CNT	1	0.664 ± 0.003	3.86 ± 0.01	0.346	66.2 ± 0.08	-
POPC-PS29x6/CNT	1	0.665 ± 0.003	3.87 ± 0.01	0.348	62.2 ± 0.06	-
POPC-PSCOOH29x2/CNT	1	0.663 ± 0.003	3.86 ± 0.01	0.348	67.2 ± 0.03	-
POPC-PSCOOH29x4/CNT	1	0.664 ± 0.003	3.86 ± 0.01	0.348	67.2 ± 0.07	-
POPC-PSCOOH29x6/CNT	1	0.666 ± 0.003	3.87 ± 0.01	0.348	62.5 ± 0.02	-
POPC-PS29x4/CNT	5	0.674 ± 0.004	3.91 ± 0.02	0.346	58.2 ± 0.05	-
POPC-PS29x6/CNT	5	0.674 ± 0.003	3.98 ± 0.02	0.334	54.6 ± 0.02	-
POPC-PSCOOH29x4/CNT	5	0.676 ± 0.004	3.89 ± 0.02	0.345	55.9 ± 0.03	-
POPC-PSCOOH29x6/CNT	5	0.676 ± 0.003	3.97 ± 0.02	0.338	56.0 ± 0.09	-
POPC/CHOL	-	0.523 ± 0.004	4.04 ± 0.02	0.399	46.6 ± 0.04	81.9 ± 0.06
POPC/CHOL-PS29x4/CNT	1	0.527 ± 0.004	4.05 ± 0.02	0.401	43.2 ± 0.05	85.5 ± 0.08
POPC/CHOL-PS29x6/CNT	1	0.528 ± 0.004	4.05 ± 0.02	0.402	43.4 ± 0.05	81.2 ± 0.05
POPC/CHOL-	1	0.527 ± 0.004	4.05 ± 0.02	0.403	46.9 ± 0.03	83.7 ± 0.06

Model						
PSCOOH29x4/CNT						
POPC/CHOL-PSCOOH29x6/CNT	1	0.528 ± 0.004	4.02 ± 0.02	0.401	47.0 ± 0.02	80.9 ± 0.04
POPC/CHOL-PS29x4/CNT	5	0.543 ± 0.005	4.06 ± 0.02	0.407	41.7 ± 0.02	73.2 ± 0.02
POPC/CHOL-PS29x6/CNT	5	0.538 ± 0.006	4.22 ± 0.02	0.387	39.4 ± 0.02	76.0 ± 0.07
POPC/CHOL-PSCOOH29x4/CNT	5	0.544 ± 0.005	4.08 ± 0.02	0.409	39.9 ± 0.05	69.2 ± 0.10
POPC/CHOL-PSCOOH29x6/CNT	5	0.539 ± 0.006	4.24 ± 0.02	0.372	42.9 ± 0.04	72.1 ± 0.04

From visual inspection, CHOL molecules are observed to move to the interior region of the bilayer, then either migrate to the other leaflet or return to the same leaflet. All successful CHOL flip-flop events detected in the last 2 μs of trajectories are listed in Table 4. While the flip-flop rates of CHOL do not change in the presence of a single nanoparticle, they decrease by about 6-12 % with 5 nanoparticles. Thus, the presence of CNTs inside the bilayer makes the rotation and translocation of CHOL more difficult. As a result of the clustering of CNTs with 6 PS or PSCOOH chains, the trans-bilayer motion of CHOL is decreased more pronouncedly. Previous studies have shown that CHOL flip-flop rates occur on a sub-millisecond timescale and are affected by temperature, CHOL concentration, bilayer order, and lipid saturation level.[93-95] When the temperature is decreased from 310 K to 290 K, lipid tail ordering increases, and the flip-flop rate decreases to one-tenth.[95] Increasing CHOL content from 20 to 40 % decreases the flip-flop rate in DPPC by orders of magnitude.[96] Moreover flip-flop rates are faster in poly-unsaturated DAPC lipid bilayers than in more saturated DPPC and POPC bilayers.[93] Calculated flip-flop rates in the literature for POPC/CHOL bilayers[93,95] are lower than our findings, however, the calculation methods, simulation types, i.e., atomistic or CG, and the temperature may play important roles in these results.

Table 4. Cholesterol (CHOL) flip-flop rates in POPC/CHOL bilayers. Values are based on the last 2 μs of trajectories.

Model	No of NP	No of Successful Flip-Flops	CHOL Flip-Flop Rate (μs⁻¹)
POPC/CHOL	-	13978	11.4
POPC/CHOL-PS29x4/CNT	1	13842	11.3
POPC/CHOL-PS29x6/CNT	1	13781	11.2
POPC/CHOL-PSCOOH29x4/CNT	1	13781	11.2
POPC/CHOL-PSCOOH29x6/CNT	1	13719	11.2
POPC/CHOL-PS29x4/CNT	5	13128	10.7

|			
POPC/CHOL-PS29x6/CNT	5	12662	10.3
POPC/CHOL-PSCOOH29x4/CNT	5	13033	10.6
POPC/CHOL-PSCOOH29x6/CNT	5	12292	10.0

The translocation of PSCNT or PSCOOHCNT across POPC or POPC/CHOL was investigated through density distribution analysis. In the presence of a single pristine/functionalized CNT, no significant changes in the properties of the lipid bilayers were observed. With 5 functionalized CNTs, density distributions of lipids (i.e., PO4 or ROH groups), water, ions, and the CNTs are presented in Figure 4. The introduction of PSCNT or PSCOOHCNT into the bilayers results in a decrease in the intensity of PO4 and/or ROH density peaks both in POPC and POPC/CHOL bilayers. This effect is more significant with CNTs with 6 PSCOOH chains in POPC/CHOL bilayer (cf. Figure 4(j)). The density peaks of CNTs in the POPC/CHOL are lower and broader than those in the POPC bilayer. In POPC/CHOL membrane, the density distributions of CNTs with 4 chains of PS or PSCOOOH are similar to each other. Likewise, the density distributions of CNTs with 6 chains of PS or PSCOOOH are similar. CHOL was also observed to translocate through interior regions of the bilayer confirming the previous findings (cf. Figure 4(f-j)). During the internalization of CNTs into the membrane, water molecules are transported to the bilayer. The open-ended structure of the CNT allows water molecules to enter the tube and be transported across the bilayer as previously reported.[27,97] In the POPC bilayer, water transport is observed with both PSCNT and PSCOOHCNT. However, not only water molecules but also ions are transported to the membrane by CNTs with 6 chains of PS or PSCOOH (c.f. Figure S7(c,e)). On the other hand, in POPC/CHOL membrane, waters and ions are observed to be present inside the bilayer only for PSCOOH functionalized CNTs (c.f. Figure S7(i,j)). It has been asserted that open-ended CNTs may also entail the penetration of lipid headgroups or lipid tails across the bilayer,[30] where the free energy barrier that must be overcome to penetrate the bilayer is lower for capped nanotubes.[98] Capped CNTs are out of the scope of this study, however, both in the POPC and POPC/CHOL membranes, CNTs with 6 chains of PS or PSCOOH are observed to be blocked by POPC lipids (c.f. Figure S7(c,e,h,j). Still, the encapsulation of a drug can inhibit the lipid blockage of nanotubes as presented in our AA study.[43]
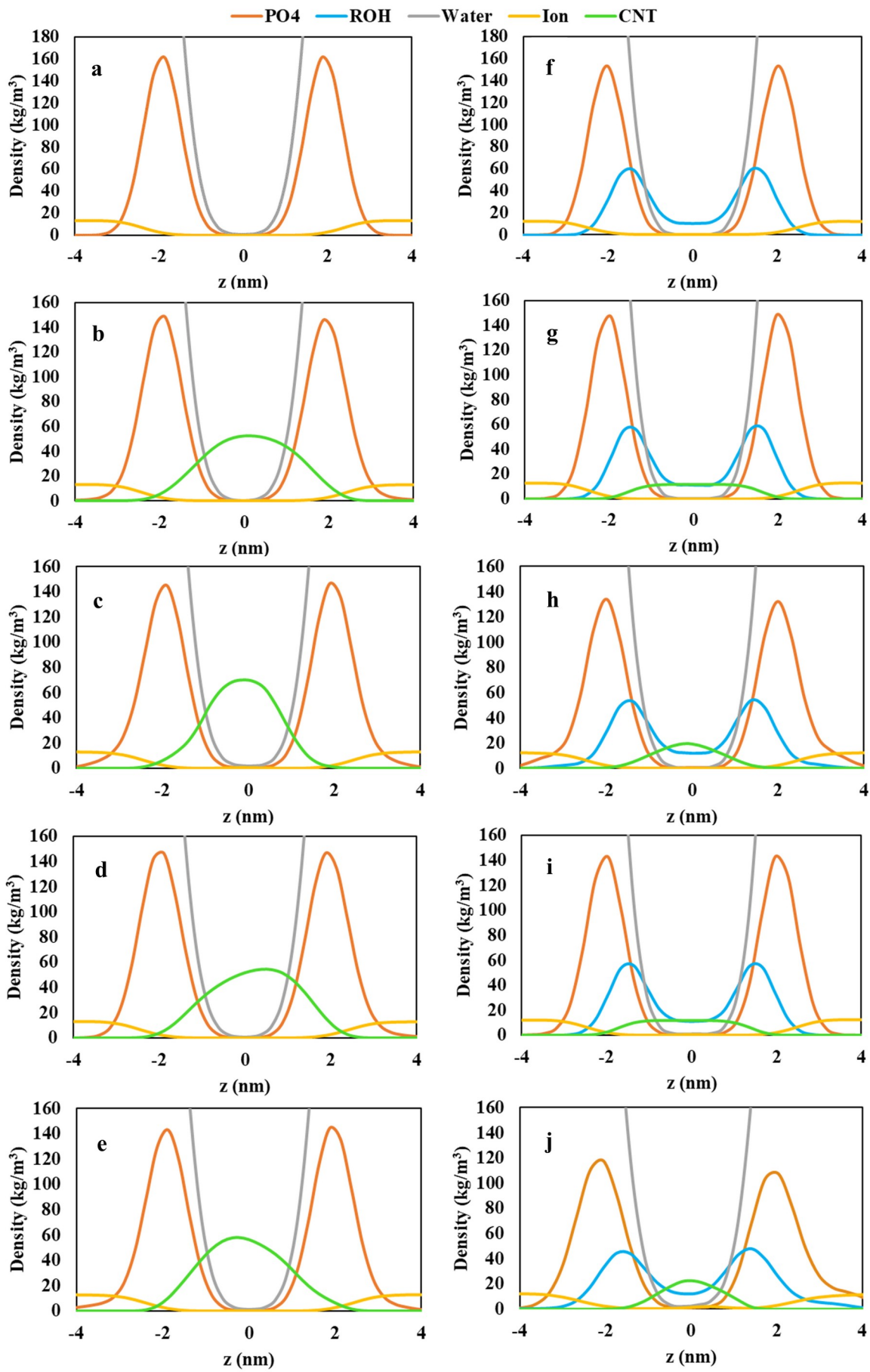
Figure 4. Density distributions of lipid phosphate (PO4) and hydroxyl (ROH) groups, and water, ion, and CNT molecules in the presence of 5 functionalized CNTs for **a)** POPC, **b)** POPC-PS29x4/CNT, **c)** POPC-PS29x6/CNT, **d)** POPC- PSCOOH29x4/CNT, **e)** POPC- PSCOOH29x6/CNT, **f)** POPC/CHOL, **g)** POPC/CHOL-PS29x4/CNT, **h)** POPC/CHOL-PS29x6/CNT, **i)** POPC/CHOL- PSCOOH29x4/CNT, **j)** POPC/CHOL- PSCOOH29x6/CNT.

The residence time spent in the aqueous phase varies from system to system and we did not find any trend with chain length or grafting density (c.f. Figure S8-S9). However, among single CNTs in POPC systems, the longest residence time in bulk water is found for CNTs that are functionalized with 96 monomers of PS or PSCOOH as ~132 and ~110 ns, respectively. With 5 functionalized CNTs, on the other hand, the longest internalization time into the POPC is recorded with 6 chains of PS as ~220 ns, while the internalization time into the POPC/CHOL membrane is ~258 ns with 6 chains of PSCOOH functional group. This is attributed to the increasing hydrophilicity of the nanotube with functional groups.[43,99]

PS and PSCOOH functionalized CNTs penetrate the membranes individually or by making clusters of two (cf. Figure 5). Once they are internalized, they form clusters of 2 or 3 and all CNTs which are functionalized with 6 polymer chains form clusters of 5 at the end of the 10 µs simulation time (cf. Figure 6.). In the POPC-CHOL system, CNTs that are modified by 4 chains of PS or PSCOOH align near parallel with the bilayer normal while the others have mixed (with 6 chains of PS) or near perpendicular (with 6 chains of PSCOOH) alignment (c.f. Figure S10).
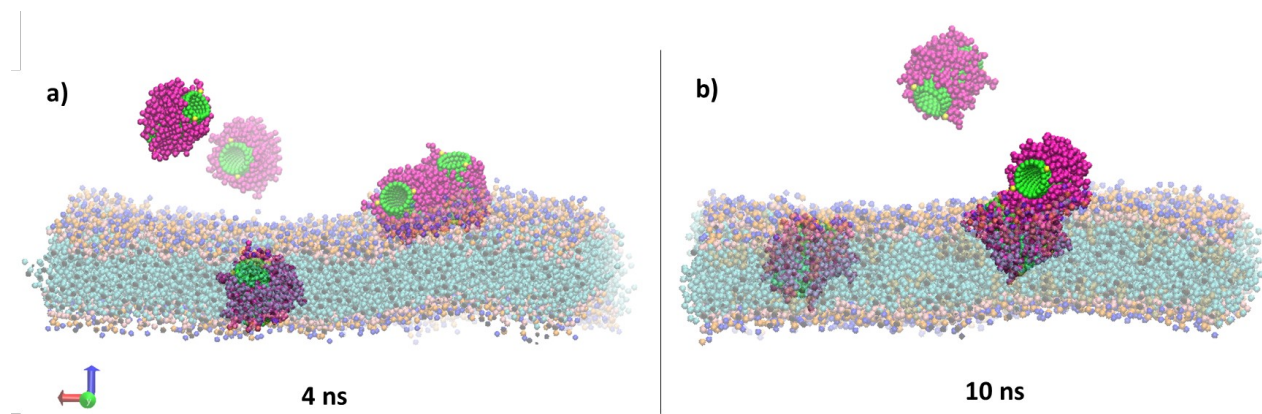

Figure 5. Internalization of PS29x4/CNT through a) POPC, b) POPC/CHOL membranes.
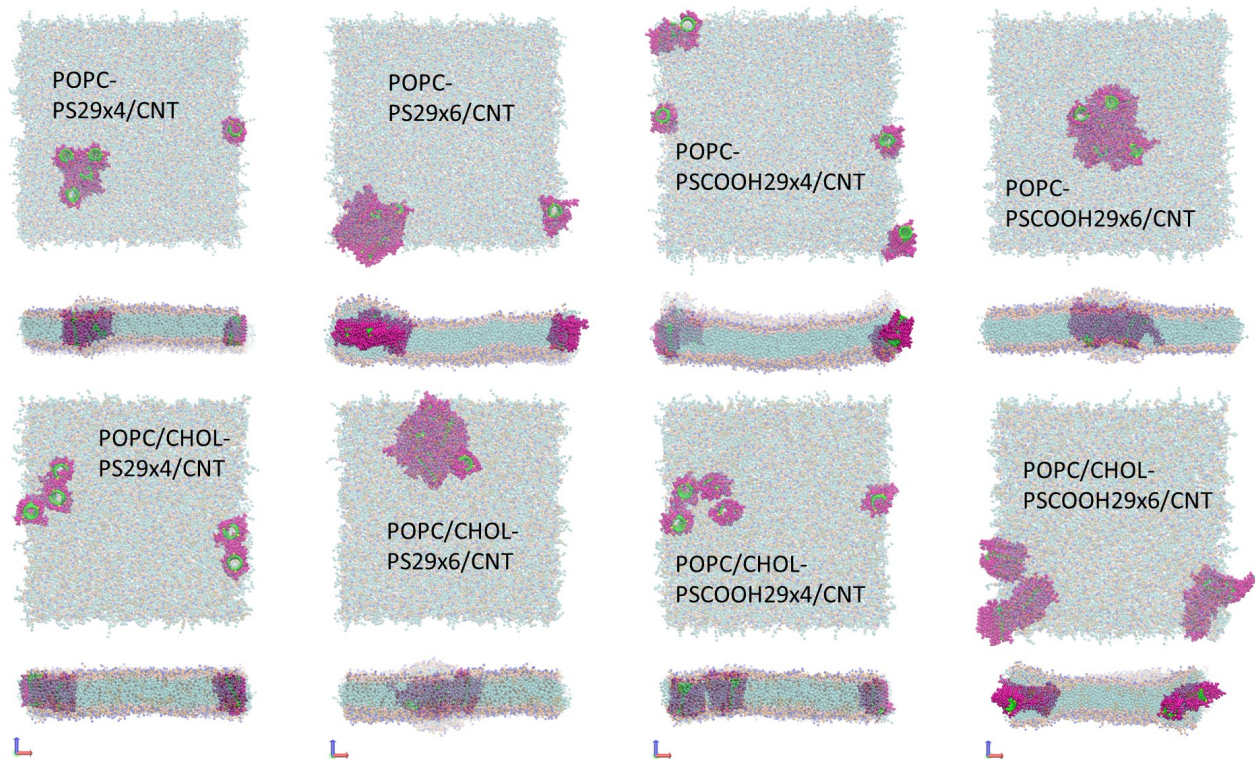
Figure 6. Top and side view of configurations taken from the trajectories at 10 µs for POPC (upper panel) and POPC/CHOL (lower panel) systems in the presence of functionalized CNTs at different grafting densities.

The radius of gyration (ROG) and carbon end-to-end (EtE) distance are two important structural descriptors of a polymer. ROG and EtE distances of PS or PSCOOH chains that are covalently linked to single CNTs are plotted in Figure 7 with changing polystyrene chain lengths. For both hydrogen and carboxyl-terminated polystyrene, ROG increases as chain length increases, confirming the previous findings in the literature.[60] EtE distances, on the other hand, increase with the increasing number of monomers in PS; while it is almost the same in PSCOOH with 29 and 48 monomers but decreases with 96 monomers. This EtE distance reduction in PSCOOH with 96 monomers can be attributed to the open carboxyl end of the PSCOOH passing inside the CNT and approaching the polar junction group.
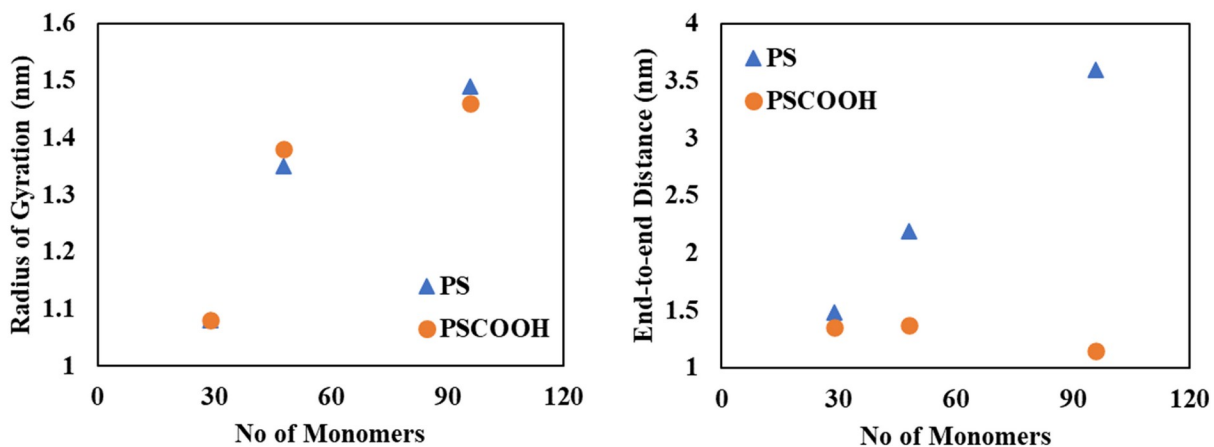
Figure 7. The average radius of gyration and end-to-end distances of PS and PSCOOH which are connected to a CNT with 29, 48, and 96 monomers. Data is taken from the last 2 μs trajectories of single functionalized CNTs in POPC membrane.

The angle distributions between the POPC bilayer normal and the long axis vector of CNT are given in Figure 8 for different PS or PSCOOH chain lengths and grafting densities. It has been reported that short CNTs with a 1.5 nm inner diameter have tilt angles between 0°-15° in the DOPC bilayer through cryogenic TEM analysis[100] and in situ SAXS calculations.[101] Using CNTs of similar size, Sullivan et al. calculated a larger tilt angle (0°-25°) by scanning AFM images across the equimolar DMPC/DOPC membrane.[102] These findings are supported here where the pristine CNT makes mostly less than 20° angle with POPC. (c.f. Figure S11) Moreover, short CNTs with ∼2 nm in length are confirmed to orient parallel to lipid molecules when embedded in a phospholipid bilayer.[103] By modifying CNTs with 29 monomers of PS or PSCOOH, we obtain similar tilt angle distributions, generally below 25°. Upon grafting 48 or 96 PS monomers, the tilting range broadens, however, the common angle ranges are similar in both. Differently, a tilt angle of about 80° is found with 96 monomers of PSCOOH attached to a CNT. Since the PSCOOH chain covers both the interior and exterior regions of CNT in this configuration, lipids cannot diffuse into the nanotube, and CNT prefers to be near-perpendicular to the bilayer normal, unlike the others that allow the lipids to diffuse inside the nanotube.

Modification of CNTs with different groups may change their configurations and polar functional groups can inhibit tilting.[75] It has been shown that hydroxyl-modified CNTs tend to be vertical to the bilayer center when the length of the CNT is shorter than the bilayer thickness.[81] However, by varying the grafting density of PSCOOH at the end of CNTs, we didn't observe a hindrance

effect. But wider tilt angle distributions were observed mostly at ~10°-20° range (cf. Figure 8(b)). This may be attributed to the amphiphilic nature of the PSCOOH model. When CNTs are functionalized with 4 chains of PS, the nanotube tilts about 60° with respect to the POPC normal due to PS blockage. Therefore, the occupation of CNTs with either PS or PSCOOH results in an increase in tilting angle with the bilayer normal.
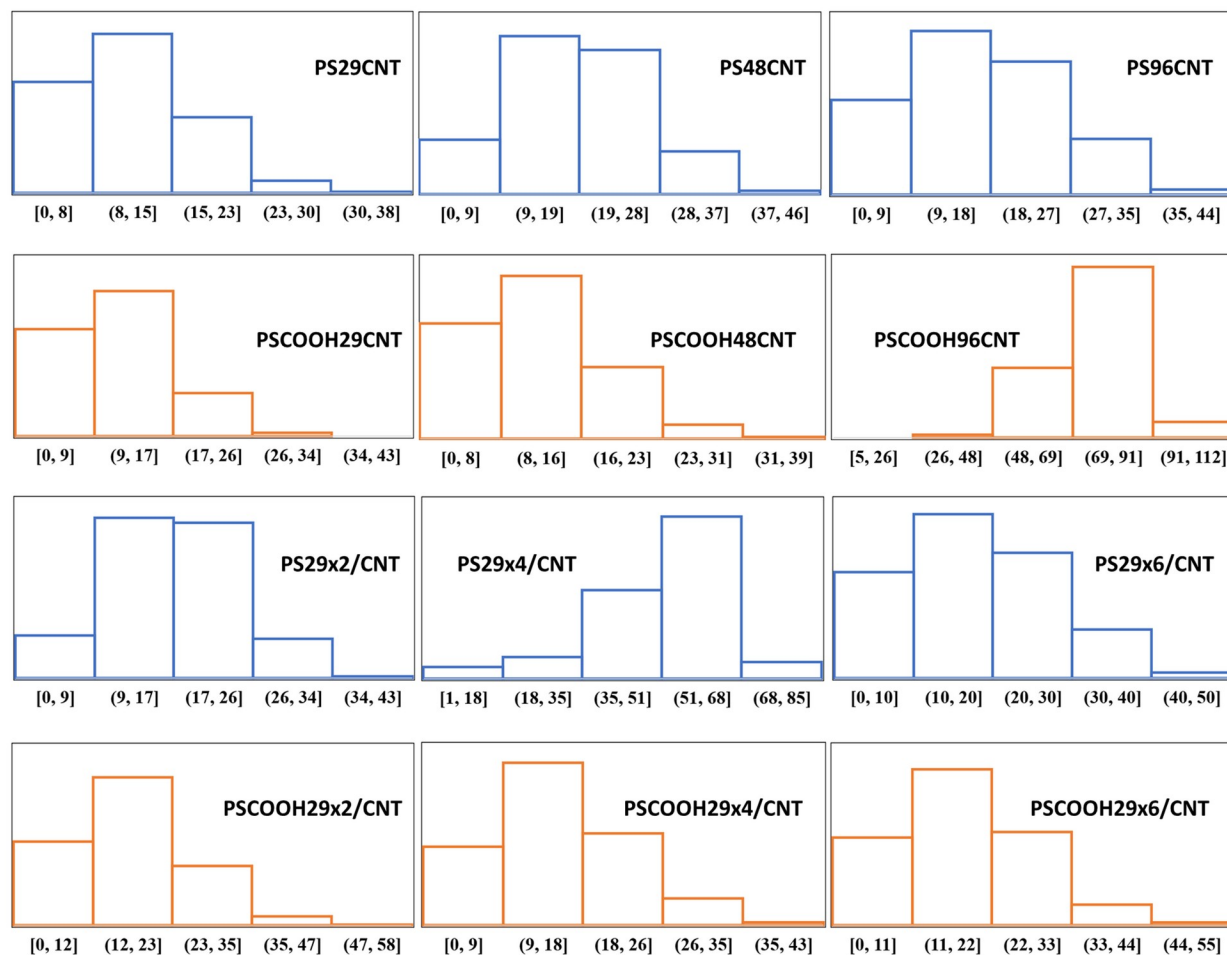
Figure 8. Distribution of angles (°) between CNT long axis and POPC bilayer normal at different chain lengths and grafting densities of PS or PSCOOH. Data is taken from the last 2 μs trajectories of single functionalized CNTs in POPC membrane.

In conclusion, Martini3 CG models of pristine and polystyrene functionalized CNTs were developed in agreement with their structural and thermodynamic properties. The developed models at different chain lengths and grafting densities of PS or PSCOOH were investigated in terms of their translocation behavior through POPC and POPC/CHOL membranes. At the studied concentrations, CNTs passively diffuse into the membranes with no physical damage to the membrane integrity. Due to the condensing effect of CHOL, the properties of lipid bilayers change, i.e., area-per-lipid and lateral diffusion constants decrease, whereas the bilayer thickness and tail order parameters increase. At increasing CNT concentrations, flip-flop rates of CHOL are reduced because of the diminished OH density in the core region of the membrane. The tilt angles between CNTs and the bilayer normal are affected by the inclusion of either lipids or polystyrene chains into the CNTs as well as by the polarity of polystyrene chains. Consequently, PS or PSCOOH-modified CNTs are shown to have the potential to be used as carrier agents in drug delivery platforms by confirming our atomistic findings.[43] But, CNT concentration, polystyrene chain length, and polystyrene grafting density are the important parameters to consider in the design of safe and controlled drug delivery. It is likely that CNTs partition into membranes affect the functionality of membrane proteins as well as altering membrane properties. It has been proposed that when nanoparticles partition into membranes they change intramembrane pressure field, resulting in changes in membrane protein functions.[104] Therefore, to understand how CNTs interact with biological membranes, the role of membrane proteins can be addressed by MD simulations. Furthermore, the toxicity of carbon nanoparticles have been associated with the generation or quench of reactive oxygen species (ROS) *in vitro* studies[105] however the factors determining their reactivity is not well described yet. In the future, our results can form the basis for the development of more complex systems, especially in the presence of drug molecules and membrane proteins, and the effect of lipid oxidation on the toxicity mechanism of CNTs may be further investigated with the developed models.

References

1.   Dai, H. 2002. Carbon nanotubes: Opportunities and challenges. *Surf. Sci.* 500:218–241.

2.   Popov, V.N. 2004. Carbon nanotubes: Properties and application. *Mater. Sci. Eng. R Reports*. 43:61–102.

3.   Liu, Z., S. Tabakman, K. Welsher, and H. Dai. 2009. Carbon nanotubes in biology and medicine: In vitro and in vivo detection, imaging and drug delivery. *Nano Res.* 2:85–120.

4.   Liu, Z., J.T. Robinson, S.M. Tabakman, K. Yang, and H. Dai. 2011. Carbon materials for drug delivery & cancer therapy. *Mater. Today*. 14:316–323.

5.   He, H., L.A. Pham-Huy, P. Dramou, D. Xiao, P. Zuo, and C. Pham-Huy. 2013. Carbon nanotubes: Applications in pharmacy and medicine. *Biomed Res. Int.* 2013.

6.   Bianco, A., K. Kostarelos, and M. Prato. 2005. Applications of carbon nanotubes in drug delivery. *Curr. Opin. Chem. Biol.* 9:674–679.

7.   Lacerda, L., S. Raffa, M. Prato, A. Bianco, and K. Kostarelos. 2007. Cell-penetrating CNTs for. *Nanotoday*. 2:38–43.

8.   Zhang, W., Z. Zhang, and Y. Zhang. 2011. The application of carbon nanotubes in target drug delivery systems for cancer therapies. *Nanoscale Res. Lett.* 6:1–22.

9.   Liu, Z., K. Chen, C. Davis, S. Sherlock, Q. Cao, X. Chen, and H. Dai. 2008. Drug delivery with carbon nanotubes for in vivo cancer treatment. *Cancer Res.* 68:6652–6660.

10.   Bhirde, A.A., V. Patel, J. Gavard, G. Zhang, A.A. Sousa, A. Masedunskas, R.D. Leapman, R. Weigert, J.S. Gutkind, and J.F. Rusling. 2009. Targeted killing of cancer cells in vivo and in vitro with EGF-directed carbon nanotube-based drug delivery. *ACS Nano*. 3:307–316.

11.   Zhang, X., L. Meng, Q. Lu, Z. Fei, and P.J. Dyson. 2009. Targeted delivery and controlled release of doxorubicin to cancer cells using modified single wall carbon nanotubes. *Biomaterials*. 30:6041–6047.

12.   Pantarotto, D., R. Singh, D. McCarthy, M. Erhardt, J.P. Briand, M. Prato, K. Kostarelos, and A. Bianco. 2004. Functionalized carbon nanotubes for plasmid DNA gene delivery. *Angew. Chemie - Int. Ed.* 43:5242–5246.

13.   Kam, N.W.S., T.C. Jessop, P.A. Wender, and H. Dai. 2004. Nanotube molecular transporters: Internalization of carbon nanotube-protein conjugates into mammalian cells. *J. Am. Chem. Soc.* 126:6850–6851.

14.   Pantarotto, D., J.P. Briand, M. Prato, and A. Bianco. 2004. Translocation of bioactive peptides across cell membranes by carbon nanotubes. *Chem. Commun.* 4:16–17.

15.   Colvin, V.L. 2004. The potential environmental impact of engineered nanomaterials. *Nat. Biotechnol.* 22:760–760.

16.   Chen, R.J., S. Bangsaruntip, K.A. Drouvalakis, N. Wong Shi Kam, M. Shim, Y. Li, W. Kim, P.J. Utz, and H. Dai. 2003. Noncovalent functionalization of carbon nanotubes for highly specific electronic biosensors. *Proc. Natl. Acad. Sci. U. S. A.* 100:4984–4989.

17.   Banerjee, S., T. Hemraj-Benny, and S.S. Wong. 2005. Covalent surface chemistry of single-walled carbon nanotubes. *Adv. Mater.* 17:17–29.

18.   Hirsch, A., and O. Vostrowsky. 2005. Functionalization of carbon nanotubes. *Top. Curr. Chem.* 245:193–237.

19.   Dumortier, H., S. Lacotte, G. Pastorin, R. Marega, W. Wei, D. Bonifazi, J.P. Briand, M. Prato, S. Muller, and A. Bianco. 2006. Functionalized carbon nanotubes are non-cytotoxic and preserve the functionality of primary immune cells. *Nano Lett.* 6:3003.

20.   Costa, P.M., M. Bourgognon, J.T.W. Wang, and K.T. Al-Jamal. 2016. Functionalized carbon nanotubes: From intracellular uptake and cell-related toxicity to systemic brain delivery. *J. Control. Release*. 241:200–219.

21.   Vardharajula, S., S.Z. Ali, P.M. Tiwari, E. Eroǧlu, K. Vig, V.A. Dennis, and S.R. Singh. 2012. Functionalized carbon nanotubes: Biomedical applications. *Int. J. Nanomedicine*. 7:5361–5374.

22.   Liu, Z., W. Cai, L. He, N. Nakayama, K. Chen, X. Sun, X. Chen, and H. Dai. 2007. In vivo biodistribution and highly efficient tumour targeting of carbon nanotubes in mice. *Nat. Nanotechnol.* 2:47–52.

23.   Liu, Z., C. Davis, W. Cai, L. He, X. Chen, and H. Dai. 2008. Circulation and long-term fate of functionalized, biocompatible single-walled carbon nanotubes in mice probed by Raman spectroscopy. *Proc. Natl. Acad. Sci. U. S. A.* 105:1410–1415.

24.   Prencipe, G., S.M. Tabakman, K. Welsher, Z. Liu, A.P. Goodwin, L. Zhang, J. Henry, and H. Dai. 2009. PEG branched polymer for functionalization of nanomaterials with ultralong blood circulation. *J. Am. Chem. Soc.* 131:4783–4787.

25.   Bhirde, A.A., Patel, S., Sousa, A.A., Patel, V., Molinolo, A.A., Ji, Y., Leapman, R.D., Gutkind, J.S., and J.F. Rusling. 2010. Distribution and clearance of PEG-single-walled carbon nanotube cancer drug delivery vehicles in mice. *Nanomed.* 5:1535–1546.

26.   Liu, X., H. Tao, K. Yang, S. Zhang, S.T. Lee, and Z. Liu. 2011. Optimization of surface chemistry on single-walled carbon nanotubes for in vivo photothermal ablation of tumors. *Biomaterials*. 32:144–151.

27.   Wallace, E.J., and M.S.P. Sansom. 2008. Blocking of carbon nanotube based nanoinjectors by lipids: A simulation study. *Nano Lett.* 8:2751–2756.

28.   Pogodin, S., and V.A. Baulin. 2010. Can a carbon nanotube pierce through a phospholipid bilayer? *ACS Nano*. 4:5293–5300.

29.   Kraszewski, S., F. Picaud, I. Elhechmi, T. Gharbi, and C. Ramseyer. 2012. How long a functionalized carbon nanotube can passively penetrate a lipid membrane. *Carbon N. Y.* 50:5301–5308.

30.   Kraszewski, S., A. Bianco, M. Tarek, and C. Ramseyer. 2012. Insertion of short amino-functionalized single-walled carbon nanotubes into phospholipid bilayer occurs by passive diffusion. *PLoS One*. 7:1–11.

31.   Baoukina, S., L. Monticelli, and D.P. Tieleman. 2013. Interaction of pristine and functionalized carbon nanotubes with lipid membranes. *J. Phys. Chem. B*. 117:12113–12123.

32.   Shen, C., G. Zou, W. Guo, and H. Gao. 2020. Lipid coating and end functionalization govern the formation and stability of transmembrane carbon nanotube porins. *Carbon N. Y.* 164:391–397.

33.   Bobadilla, A.D., E.L.G. Samuel, J.M. Tour, and J.M. Seminario. 2013. Calculating the hydrodynamic volume of poly(ethylene oxylated) single-walled carbon nanotubes and hydrophilic carbon clusters. *J. Phys. Chem. B*. 117:343–354.

34.   Lee, H. 2013. Molecular dynamics studies of pegylated single-walled carbon nanotubes: The effect of PEG size and grafting density. *J. Phys. Chem. C*. 117:26334–26341.

35.   Ham, H.T., Koo, C.M., Kim, S.O., Choi, S., and I.J. Chung. 2004. Chemical modification of carbon nanotubes and preparation of polystyrene/carbon nanotubes composites. *Macromol. Res.* 12:384–390.

36.   Huang, H.M., Liu, I.C., Chang, C.Y.U., Tsai, H.C., Hsu, C.H., and R.C.C. Tsiang. 2004. Preparing a polystyrene-functionalized multiple-walled carbon nanotubes via covalently linking acyl chloride functionalities with living polystyryllithium. *J. Polym. Sci. Part A Polym. Chem*. 42:5802–5810.

37.   Li, H., Cheng, F., Duft, A.M., and A. Adronov. 2005. Functionalization of single-walled carbon nanotubes with well-defined polystyrene by "click" coupling. *J. Am. Chem. Soc*. 127:14518–14524.

38.   Yang, Y., Xie, X., Wu, J., and Y.W. Mai. 2006. Synthesis and self-assembly of polystyrene-grafted multiwalled carbon nanotubes with a hairy-rod nanostructure. *J. Polym. Sci. A Polym. Chem*. 44: 3869–3881.

39.   Fragneaud, B., K. Masenelli-Varlot, A. Gonzalez-Montiel, M. Terrones, and J.Y. Cavaillé. 2008. Mechanical behavior of polystyrene grafted carbon nanotubes/polystyrene nanocomposites. *Compos. Sci. Technol.* 68:3265–3271.

40.   Chadwick, R.C., U. Khan, J.N. Coleman, and A. Adronov. 2013. Polymer grafting to single-walled carbon nanotubes: Effect of chain length on solubility, graft density and mechanical properties of macroscopic structures. *Small*. 9:552–560.

41.   Tabet, L., C. Bussy, A. Setyan, A. Simon-Deckers, M.J. Rossi, J. Boczkowski, and S. Lanone. 2011. Coating carbon nanotubes with a polystyrene-based polymer protects against pulmonary toxicity. *Part. Fibre Toxicol.* 8:1–13.

42.   Gul, G., R. Yildirim, and N. Ileri-Ercan. 2021. Cytotoxicity analysis of nanoparticles by association rule mining. *Environ. Sci. Nano*. 8:937–949.

43.   Gul, G., R. Faller, and N. Ileri-Ercan. 2022. Polystyrene-modified carbon nanotubes: Promising carriers in targeted drug delivery. *Biophys. J.* 121:4271–4279.

44.   Berendsen, H.J.C., D. van der Spoel, and R. van Drunen. 1995. GROMACS: A message-passing parallel molecular dynamics implementation. *Comput. Phys. Commun.* 91:43–56.

45.   Humphrey, W., A. Dalke, and K. Schulten. 1996. VMD: Visual Molecular Dynamics. *J. Mol. Graph.* 14:33–38.

46.   Jo, S., Kim, T., Iyer, V.G., and W. Im. 2008. CHARMM-GUI: A Web-based Graphical User Interface for CHARMM. *J. Comput. Chem.* 29:1859–1865.

47.   Czerw, R., Z. Guo, P.M. Ajayan, Y.P. Sun, and D.L. Carroll. 2001. Organization of polymers onto carbon nanotubes: a route to nanoscale assembly. *Nano Lett.* 1:423–427.

48.   Huang, W., Y. Lin, S. Taylor, J. Gaillard, A.M. Rao, and Y.P. Sun. 2002. Sonication-Assisted Functionalization and Solubilization of Carbon Nanotubes. *Nano Lett.* 2:231–234.

49.   Pramanik, C., J.R. Gissinger, S. Kumar, and H. Heinz. 2017. Carbon Nanotube Dispersion in Solvents and Polymer Solutions: Mechanisms, Assembly, and Preferences. *ACS Nano*. 11:12805–12816.

50.   Vanommeslaeghe, K., E. Hatcher, C. Acharya, S. Kundu, S. Zhong, J. Shim, E. Darian, O. Guvench, P. Lopes, I. Vorobyov, and A.D. MacKerell Jr. 2010. CHARMM General Force Field (CGenFF): A force field for drug-like molecules compatible with the CHARMM all-atom additive biological force fields. *J. Comput. Chem.* 31:671–690.

51.   Bussi, G., D. Donadio, and M. Parrinello. 2007. Canonical sampling through velocity rescaling. *J. Chem. Phys.* 126.

52.   Darden, T., D. York, and L. Pedersen. 1993. Particle mesh Ewald: An N·log(N) method for Ewald sums in large systems. *J. Chem. Phys.* 98:10089–10092.

53.   Parrinello, M., and A. Rahman. 1981. Polymorphic transitions in single crystals: A new molecular dynamics method. *J. Appl. Phys.* 52:7182–7190.

54.   Hess, B., H. Bekker, H.J.C. Berendsen, and J.G.E.M. Fraaije. 1997. LINCS: A Linear Constraint Solver for molecular simulations. *J. Comput. Chem.* 18:1463–1472.

55.   Marrink, S.J., H.J. Risselada, S. Yefimov, D.P. Tieleman, and A.H. De Vries. 2007. The MARTINI force field: Coarse grained model for biomolecular simulations. *J. Phys. Chem. B*. 111:7812–7824.

56.   Souza, P.C.T., R. Alessandri, J. Barnoud, S. Thallmair, I. Faustino, F. Grünewald, I. Patmanidis, H. Abdizadeh, B.M.H. Bruininks, T.A. Wassenaar, P.C. Kroon, J. Melcr, V. Nieto, V. Corradi, H.M. Khan, J. Domański, M. Javanainen, H. Martinez-Seara, N. Reuter, R.B. Best, I. Vattulainen, L. Monticelli, X. Periole, D.P. Tieleman, A.H. de Vries, and S.J. Marrink. 2021. Martini 3: a general purpose force field for coarse-grained molecular dynamics. *Nat. Methods*. 18:382–388.

57.   Alessandri, R., J. Barnoud, A.S. Gertsen, I. Patmanidis, A.H. de Vries, P.C.T. Souza, and S.J. Marrink. 2021. Martini 3 Coarse-Grained Force Field: Small Molecules. 1–48.

58.   Barnoud, J. CG Builder. https://jbarnoud.github.io/cgbuilder/ (accessed at September 2021).

59.   Grünewald, F., R. Alessandri, P.C. Kroon, L. Monticelli, P.C.T. Souza, and S.J. Marrink. 2022. Polyply; a python suite for facilitating simulations of macromolecules and nanomaterials. *Nat. Commun.* 13:1–12.

60.   Rossi, G., L. Monticelli, S.R. Puisto, I. Vattulainen, and T. Ala-Nissila. 2011. Coarse-graining polymers with the MARTINI force-field: Polystyrene as a benchmark case. *Soft Matter*. 7:698–708.

61.   Berendsen, H.J.C., J.P.M. Postma, W.F. Van Gunsteren, A. Dinola, and J.R. Haak. 1984. Molecular dynamics with coupling to an external bath. *J. Chem. Phys.* 81:3684–3690.

62.   Tironi, I.G., R. Sperb, P.E. Smith, and W.F. Van Gunsteren. 1995. A generalized reaction field method for molecular dynamics simulations. *J. Chem. Phys.* 102:5451–5459.

63.   Van Der Spoel, D., and P.J. Van Maaren. 2006. The origin of layer structure artifacts in simulations of liquid water. *J. Chem. Theory Comput*. 2:1–11.

64.   Bennett, C.H. 1976. Efficient estimation of free energy differences from Monte Carlo data. *J. Comput. Phys.* 22:245–268.

65.   Leach, A.R. 2001. Molecular Modelling Principles and Applications. 2nd ed. Prentice Hall.

66.   Beutler, T.C., A.E. Mark, R.C. van Schaik, P.R. Gerber, and W.F. Van Gunsteren. 1994. Avoiding singularities and numerical instabilities in free energy calculations based on molecular simulations. *Chem. Phys. Lett.* 222:529–539.

67.   Torrie, J., and G.M. Valleau. 1977. Nonphysical sampling distributions in monte carlo free-energy estimation: umbrella sampling. *J. Comput. Phys*. 23:187-199.

68.   Kumar, S., J.M. Rosenberg, D. Bouzida, R.H. Swendsen, and P.A. Kollman. 1992. THE weighted histogram analysis method for free-energy calculations on biomolecules. I. The method. *J. Comput. Chem.* 13:1011–1021.

69.   Hub, J.S., B.L. De Groot, and D. Van Der Spoel. 2010. G-whams-a free Weighted Histogram Analysis implementation including robust error and autocorrelation estimates. *J. Chem. Theory Comput.* 6:3713–3720.

70.   Buchoux, S. 2017. FATSLiM: A fast and robust software to analyze MD simulations of membranes. *Bioinformatics*. 33:133–134.

71.   Smith, P., and C.D. Lorenz. 2021. LiPyphilic: A python toolkit for the analysis of lipid membrane simulations. *J. Chem. Theory Comput.* 17:5907–5919.

72.   Van Rossum, G., and F.L. Drake Jr. 1995. Python reference manual. Centrum voor Wiskunde en Informatica Amsterdam.

73.   Ileri Ercan, N. 2019. Understanding interactions of curcumin with lipid bilayers: a coarse-grained molecular dynamics study. *J. Chem. Inf. Model.* 59:4413–4426.

74.   MATLAB. (2018). 9.7.0.1190202 (R2019b). Natick, Massachusetts: The MathWorks Inc.

75.   Vögele, M., J. Köfinger, and G. Hummer. 2018. Molecular dynamics simulations of carbon nanotube porins in lipid bilayers. *Faraday Discuss.* 209:341–358.

76.   Bannan, C.C., G. Calabró, D.Y. Kyu, and D.L. Mobley. 2016. Calculating partition coefficients of small molecules in octanol/water and cyclohexane/water. *J. Chem. Theory Comput.* 12:4015–4024.

77.   Chaban, V. V., and E.E. Fileti. 2016. Free energy of solvation of carbon nanotubes in pyridinium-based ionic liquids. *Phys. Chem. Chem. Phys.* 18:20357–20362.

78.   Fileti, E., and V. V. Chaban. 2017. Solubility origin at the nanoscale: Enthalpic and entropic contributions in polar and nonpolar environments. *Phys. Chem. Chem. Phys.* 19:3903–3910.

79.   Toropov, A.A., D. Leszczynska, and J. Leszczynski. 2007. Predicting water solubility and octanol water partition coefficient for carbon nanotubes based on the chiral vector. *Comput. Biol. Chem.* 31:127–128.

80.   Torrens, F., and G. Castellano. 2011. (Co-)solvent selection for single-wall carbon nanotubes: Best solvents, acids, superacids and guest–host inclusion complexes. *Nanoscale.* 3:2494–2510.

81.   Gao, Y., D. Mao, J. Wu, X. Wang, Z. Wang, G. Zhou, L. Chen, J. Chen, and S. Zeng. 2019. Carbon nanotubes translocation through a lipid membrane and transporting small hydrophobic and hydrophilic molecules. *Appl. Sci.* 9.

82.   Kučerka, N., S. Tristram-Nagle, and J.F. Nagle. 2006. Structure of fully hydrated fluid phase lipid bilayers with monounsaturated chains. *J. Membr. Biol.* 208:193–202.

83.   Kučerka, N., M.P. Nieh, and J. Katsaras. 2011. Fluid phase lipid areas and bilayer thicknesses of commonly used phosphatidylcholines as a function of temperature. *Biochim. Biophys. Acta - Biomembr.* 1808:2761–2771.

84.   Plesnar, E., W.K. Subczynski, and M. Pasenkiewicz-Gierula. 2012. Saturation with cholesterol increases vertical order and smoothes the surface of the phosphatidylcholine bilayer: A molecular simulation study. *Biochim. Biophys. Acta - Biomembr.* 1818:520–529.

85.   Shahane, G., W. Ding, M. Palaiokostas, and M. Orsi. 2019. Physical properties of model biological lipid bilayers: insights from all-atom molecular dynamics simulations. *J. Mol. Model.* 25:1–13.

86.   Falck, E., M. Patra, M. Karttunen, M.T. Hyvönen, and I. Vattulainen. 2005. Response to comment by Almeida et al.: Free area theories for lipid bilayers - Predictive or not? *Biophys. J.* 89:745–752.

87.   Róg, T., M. Pasenkiewicz-Gierula, I. Vattulainen, and M. Karttunen. 2009. Ordering effects of cholesterol and its analogues. *Biochim. Biophys. Acta - Biomembr.* 1788:97–121.

88.   Olsen, B.N., A.A. Bielska, T. Lee, M.D. Daily, D.F. Covey, P.H. Schlesinger, N.A. Baker, and D.S. Ory. 2013. The structural basis of cholesterol accessibility in membranes. *Biophys. J.* 105:1838–1847.

89.   Arnarez, C., J.J. Uusitalo, M.F. Masman, H.I. Ingólfsson, D.H. De Jong, M.N. Melo, X. Periole, A.H. De Vries, and S.J. Marrink. 2015. Dry martini, a coarse-grained force field for lipid membrane simulations with implicit solvent. *J. Chem. Theory Comput.* 11:260–275.

90.   Melo, M.N., H.I. Ingólfsson, and S.J. Marrink. 2015. Parameters for Martini sterols and hopanoids based on a virtual-site description. *J. Chem. Phys.* 143.

91.   Filippov, A., G. Orädd, and G. Lindblom. 2003. Influence of cholesterol and water content on phospholipid lateral diffusion in bilayers. *Langmuir*. 19:6397–6400.

92.   Filippov, A., G. Orädd, and G. Lindblom. 2003. The effect of cholesterol on the lateral diffusion of phospholipids in oriented bilayers. *Biophys. J.* 84:3079–3086.

93.   Jo, S., H. Rui, J.B. Lim, J.B. Klauda, and W. Im. 2010. Cholesterol flip-flop: Insights from free energy simulation studies. *J. Phys. Chem. B*. 114:13342–13348.

94.   Bennett, W.F.D., and D.P. Tieleman. 2012. Molecular simulation of rapid translocation of cholesterol, diacylglycerol, and ceramide in model raft and nonraft membranes. *J. Lipid Res.* 53:421–429.

95.   Gu, R.X., S. Baoukina, and D.P. Tieleman. 2019. Cholesterol flip-flop in heterogeneous membranes. *J. Chem. Theory Comput.* 15:2064–2070.

96.   Bennett, W.F.D., J.L. MacCallum, and P. Tieleman. 2009. Thermodynamic analysis of the effect of cholesterol on dipalmitoylphosphatidylcholine lipid membranes. *J. Am. Chem. Soc.* 131:1972–1978.

97.   Lopez, C.F., S.O. Nielsen, B. Ensing, P.B. Moore, and M.L. Klein. 2005. Structure and dynamics of model pore insertion into a membrane. *Biophys. J.* 88:3083–3094.

98.   Raczyński, P., K. Górny, M. Pabiszczak, and Z. Gburski. 2013. Nanoindentation of biomembrane by carbon nanotubes - MD simulation. *Comput. Mater. Sci.* 70:13–18.

99.   Gul, G., and N. Ileri-Ercan. 2021. Fullerene translocation through peroxidized lipid membranes. *RSC Adv.* 11:7575–7586.

100.   Geng, J., K. Kim, J. Zhang, A. Escalada, R. Tunuguntla, L.R. Comolli, F.I. Allen, A. V. Shnyrova, K.R. Cho, D. Munoz, Y.M. Wang, C.P. Grigoropoulos, C.M. Ajo-Franklin, V.A. Frolov, and A. Noy. 2014. Stochastic transport through carbon nanotubes in lipid bilayers and live cell membranes. *Nature*. 514:612–615.

101.   Tran, I.C., R.H. Tunuguntla, K. Kim, J.R.I. Lee, T.M. Willey, T.M. Weiss, A. Noy, and T. Van Buuren. 2016. Structure of carbon nanotube porins in lipid bilayers: An in situ small-angle X-ray scattering (SAXS) study. *Nano Lett.* 16:4019–4024.

102.   Sullivan, K., Y. Zhang, J. Lopez, M. Lowe, and A. Noy. 2020. Carbon nanotube porin diffusion in mixed composition supported lipid bilayers. *Sci. Rep.* 10:1–8.

103.   Höfinger, S., M. Melle-Franco, T. Gallo, A. Cantelli, M. Calvaresi, J.A.N.F. Gomes, and F. Zerbetto. 2011. A computational analysis of the insertion of carbon nanotubes into cellular membranes. *Biomaterials*. 32:7079–7085.

104.   Samuli Ollila, O.H., Risselada, H.J., Louhivuori, M., Lindahl, E., Vattulainen, I. and S.J. Marrink. 2009. 3D pressure field in lipid membranes and membrane-protein complexes. *Phys. Rev. Lett*. 102:078101.

105.   Markovic, Z., and V. Trajkovic. 2008. Biomedical potential of the reactive oxygen species generation and quenching by fullerenes (C60). *Biomaterials*. 29:3561–3573.

AUTHOR INFORMATION

Corresponding Authors

[*]Nazar Ileri-Ercan. E-mail: nazar.ileri@boun.edu.tr

ORCID

Nazar Ileri-Ercan: 0000-0003-2251-1859

Roland Faller: 0000-0001-9946-3846

Gulsah Gul: 0000-0003-4469-9709

AUTHOR CONTRIBUTIONS

G. G. helped design the project, carried out simulations and simulation analysis and wrote the article. R. F. helped design the project and supervised the simulations and simulation analysis and helped write the article. N. I. E. designed the project and supervised the simulations and simulation analysis and helped write the article.

Declaration of Interests

The authors declare no competing financial interests.